Pergamon

Chaos, Solitons & Fractals Vol. 5, No. 11, pp. 2145–2152, 1995

0960–0779/95$9.50 + 0.00

0960–0779(94)00223–1

A Numerical Study of Some Fractal Properties of Riemann's 'Non-differentiable' Function

M. STIASSNIE*

Department of Engineering Mathematics, University of Bristol, UK

and

A. HADAD

Department of Environmental Sciences, The Weizmann Institute of Science, Rehovot, Israel

(*Received* 1 *October* 1994)

Abstract—The fractal dimensions, D_b and the multifractal singularity distribution functions, $F(\alpha)$ for Riemann's 'non-differentiable' functions are calculated numerically and presented here for the first time. The new fractal results are discussed through comparison with some analytically known properties of Riemann's functions. Almost all analytical properties are revealed in our numerical results.

1. INTRODUCTION

In a recent paper, Holschneider and Tchamitchian (1991) survey and extend the known properties of Riemann's 'non-differentiable' function

$$R_\mu(x) = \sum_{m=1}^{\infty} m^{-2\mu} e^{i\pi m^2 x}, \qquad \text{for } \mu > \tfrac{1}{2}. \tag{1}$$

The original function of Riemann is the imaginary part of R_1. Holschneider and Tchamitchian use wavelet transform techniques to show that the function R_μ has the following properties.

(1) R_μ is not differentiable at any irrational point for any $\mu \in (\frac{1}{2}, \frac{5}{4})$.
(2) R_μ satisfies uniformly a Hölder condition with regularity exponent $(\mu - \frac{1}{2})$ for $\mu \in (\frac{1}{2}, \frac{3}{2})$.
(3) R_μ is differentiable on the dense set of points given by $x = (2P + 1)/(2Q + 1)$, P, Q integers, for $\mu > \frac{3}{4}$.

For technical details and for a historical review of the topic the reader is referred to Holschneider and Tchamitchian [1].

The above properties assure the multifractal nature of the graphs of the real and imaginary parts of R_μ, denoted by C and S:

$$C_\mu(x) = \sum_{m=1}^{\infty} m^{-2\mu} \cos(\pi m^2 x), \qquad \text{for } \mu > \tfrac{1}{2} \tag{2}$$

*On leave from the Department of Civil Engineering, Technion, Haifa, Israel, 32000.

$$S_\mu(x) = \sum_{m=1}^{\infty} m^{-2\mu} \sin(\pi m^2 x), \qquad \text{for } \mu > \tfrac{1}{2}. \tag{3}$$

Properties (1) and (3) demonstrate the diversity in the local structure of Riemann's function. One can express the local behaviour in terms of a Lipschitz–Hölder (LH) exponent $\alpha(x)$. This LH exponent α (at a point x) is related to the maximum range Δ of a continuous function $y(x)$ at the vicinity of the point x through:

$$\lim_{\delta \to 0} \Delta(x, \delta) \propto \delta^\alpha \tag{4}$$

where

$$\Delta(x, \delta) = \sup |y(t) - y(u)| \qquad \text{for } x \leqslant t, u < x + \delta. \tag{4a}$$

The interpretation of the $\propto$ sign in (4) is rather wide. One may replace (4) by:

$$\lim_{\delta \to 0} \Delta(x, \delta) = c(x, \ln \delta).\delta^\alpha \tag{5}$$

where c can sometimes be a converging Fourier series of $(\ln \delta)$ with x dependent coefficients; thus c can oscillate wildly as δ approaches zero. An example of this type of behaviour for the Weierstrass function near the origin is shown in West [2, p. 78].

In this note, we concentrate on numerical calculations of some fractal properties of C and S, by using a box counting technique which we explain in Section 2. The results and their interpretation are given in Section 3 in light of the above properties.

2. NUMERICAL PROCEDURE

We start by dividing the domain $[0, 2]$ of the x-axis into $n_{\max}$ equal segments of length

$$\delta_{\min} = 2{n_{\max}}^{-1},$$

and denote

$$x_j = j\delta_{\min}, \qquad j = 0, 1, \ldots, n_{\max}.$$

Then we truncate (2) and (3) at some large m so that $m^{-2\mu} = \varepsilon$ and calculate values $C(x_j)$ (or $S(x_j)$) at the above points. These values will serve as our data base for all further computations. For the present note we choose $\varepsilon = 0.001$ and $n_{\max} = 2048 = 2^{11}$.

In the sequel analyses we use δ-by-δ squares and use the notation $\delta \to 0$. In practice, we have used the following decreasing series of δ values: $\delta = 1, 2^{-1}, 2^{-2}, \ldots, 2^{-9} = 2\delta_{\min}$. From (4a) we can see that the number of δ-by-δ squares which is needed to cover any function between x_i and $x_i + \delta$, where $x_i = i\delta$, is $\Delta(x_i, \delta)/\delta$. Note that i attains values from 0 to $(n - 1)$ where $n = \delta^{-1}$. Thus, the total number of squares $N(\delta)$ which is needed to completely cover the function is $\sum_{i=0}^{n-1} \Delta(x_i, \delta)/\delta$. The box-counting dimension D_b is defined and exists only when the following measure M is finite:

$$M = \lim_{\delta \to 0} \delta^{D_b - 1} \sum_{i=0}^{n-1} \Delta(x_i, \delta). \tag{6}$$

D_b is obtained from the slope of the graph of $\log N$, where $N(\delta) = \delta^{-1}\{\sum_{i=0}^{n-1} \Delta(x_i, \delta)\}$, plotted as a function of $-\log\{\delta\}$ for small enough values of δ.

As already mentioned, the local behaviour of the function $y(x)$, in terms of its Lipschitz–Hölder (LH) exponent α, is represented by:

$$\Delta(x_i, \delta) \propto \delta^\alpha \tag{7}$$

where $1 - \alpha$ determines the singularity strength. For complicated functions like C_μ (and S_μ) one would expect to have different values of α at different locations. Actually, C_μ is characterized by a union of an infinite number of subsets each related to a typical singularity α and supported on a dust in $[0, 2]$ with a fractal dimension $F(\alpha)$. The $F(\alpha)$ curve which summarizes the multifractal properties, is our main goal.

We assume that the number of squares which is needed to cover the dusts in $[0, 2]$ with LH exponent between α and $\alpha + d\alpha$ is

$$N(\alpha, \delta) \propto \delta^{-F(\alpha)} d\alpha. \tag{8}$$

A more general measure than that in (6) is the q-measure, which is given by

$$M_q = \lim_{\delta \to 0} \delta^{\tau(q)} \sum_{i=0}^{n-1} \mu_i^q \tag{9}$$

where $\tau(q)$ are sometimes called the 'mass exponents' and μ_i, which denotes the relative weight in the ith segment, is defined as

$$\mu_i = \Delta(x_i, \delta) / \sum_{i=0}^{n-1} \Delta(x_i, \delta). \tag{10}$$

Note that one can compute $\sum_{i=0}^{n-1} \mu_i^q$ for decreasing values of δ. The plot $\log N(\delta, q)$ where $N(\delta, q) = \{\sum_{i=0}^{n-1} \mu_i^q\}$ against $-\log\{\delta\}$ serves to obtain $\tau(q)$, for a given q.

From equations (6), (7) and (10), we get an expression for the relative weight in a segment as a function of its LH exponent and of the box-counting dimension:

$$\mu(\alpha, \delta) \propto \delta^{\alpha + D_b - 1}. \tag{11}$$

Using equations (8) and (11) we can write the q-measure in the form

$$M_q \propto \lim_{\delta \to 0} \int_0^\infty d\alpha \delta^{-F(\alpha) + (\alpha + D_b - 1)q + \tau(q)}. \tag{12}$$

The integral in equation (12) is calculated by the steepest descent approximation. In the limit of small δ this integral is dominated by

$$M_q \propto \delta^{-F(\alpha) + (\alpha + D_b - 1)q + \tau(q)}; \ \alpha = \alpha(q) \tag{13}$$

where α in equation (13) is the solution of $F'(\alpha) = q$, provided that $F''(\alpha) < 0$. The measure M_q in equation (13) is finite only when

$$F(\alpha) = (\alpha + D_b - 1)q + \tau(q). \tag{14}$$

Taking the derivative of equation (14) with respect to q, we find

$$\alpha = 1 - D_b - d\tau(q)/dq. \tag{15}$$

The couple of equations (14) and (15) enables us to calculate the $F(\alpha)$ curve from the mass exponents curve $\tau(q)$ and the fractal dimensions D_b which are already known.

3. RESULTS AND DISCUSSION

The fractal dimensions D_b of the curves C_μ and S_μ were calculated first and are presented in Fig. 1(a). Both curves in this figure represent monotically decreasing functions of μ. The fractal dimension of C_μ, given by the open circles, decreases from $D_b = 1.51 \pm 0.03$ at $\mu = 0.5$, to $D_b = 1 \pm 0.03$ at $\mu = 1.5$. The fractal dimension of S_μ,

denoted by full circles, is somewhat larger; it decreases from $D_b = 1.54 \pm 0.03$ at $\mu = 0.5$ to $D_b = 1 \pm 0.03$ at $\mu = 1.5$. Note that in cases where the computed values of D_b for C_μ and S_μ were the same, only open circles are presented.

As already mentioned, D_b is obtained from the slope of the graph $\log_2 N(\delta)$ plotted as a function of $-\log_2(\delta)$. To demonstrate this procedure, we give in Fig. 1(b) the results for $C_{0.75}$, $C_{1.0}$ and $C_{1.25}$; other results, for different $\mu's$ or for S_μ are of about the same quality. For the calculation of the best straight lines in Fig. 1(b) we have ignored the extreme data points which correspond to $\delta = 1$ and $\delta = 2^{-9}$. In Fig. 2(a) and (b) we show the multifractal singularity distribution $F(\alpha)$ for C_μ and S_μ, respectively, and $\mu = 0.75$, 1.0, 1.25. Note that $\alpha < 1$ is related to the set of points on the segment $0 \leqslant x < 2$ where the function has no derivative (i.e. the derivative $\to \pm \infty$) whereas $\alpha > 1$ is related to points with a vanishing derivative. The left branches of C_μ (in Fig. 2(a)), are rather similar to their counterparts for S_μ (in Fig. 2(b)); whereas the right branches are significantly different. This difference is also evident from comparing Fig. 2(c) and (d) which were used to calculate the 'mass exponents' $\tau(q)$ given by the slopes of the straight lines. The right branch of a $F(\alpha)$ curve

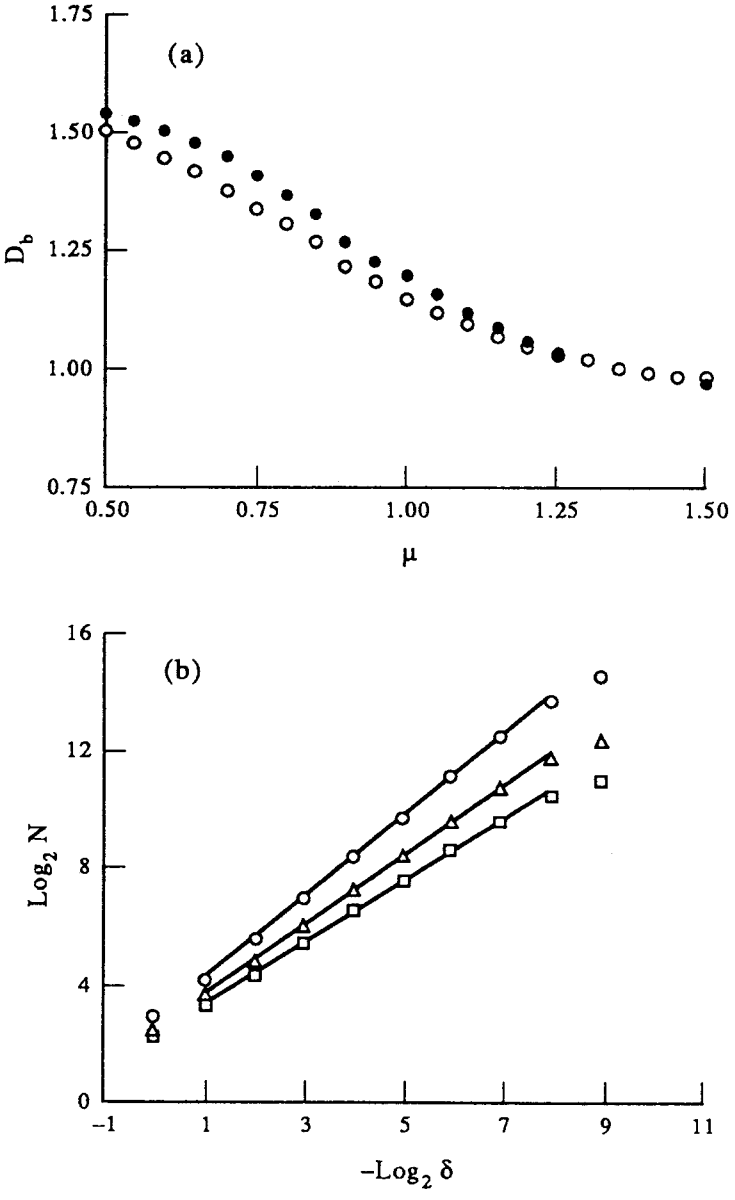

Fig. 1. (a) The fractal dimension D_b as a function of μ for C_μ ○ ○ ○, and S_μ ● ● ●. (b) $\text{Log}_2 N$ as a function of $-\text{Log}_2 \delta$ for C_μ, $\mu = 0.75$ ○ ○ ○, 1.0 △ △ △, and 1.25 □ □ □.

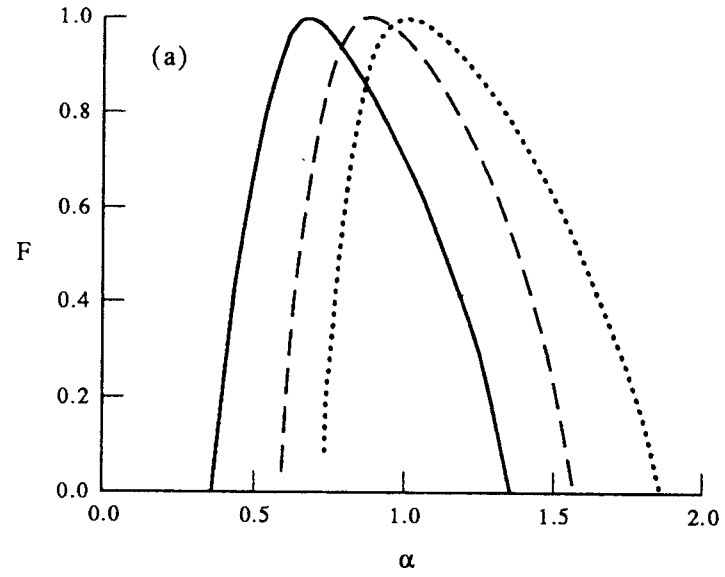
(a)
F
α
1.0
0.8
0.6
0.4
0.2
0.0
0.0
0.5
1.0
1.5
2.0

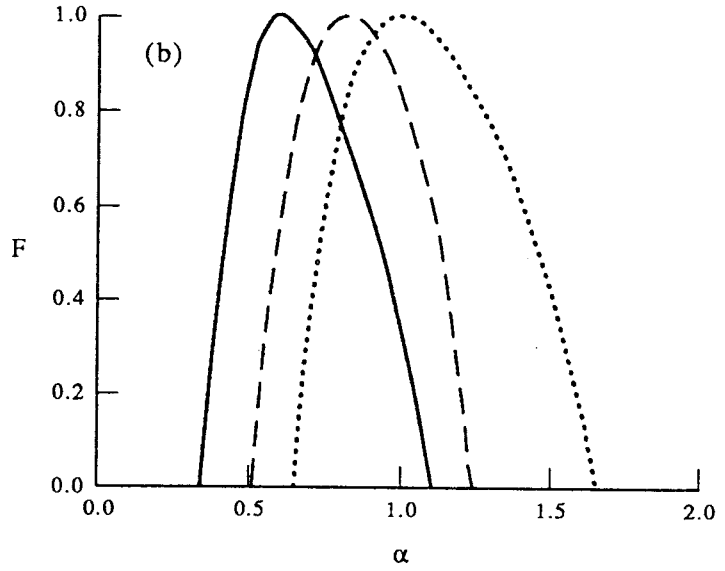
(b)
F
α
1.0
0.8
0.6
0.4
0.2
0.0
0.0
0.5
1.0
1.5
2.0

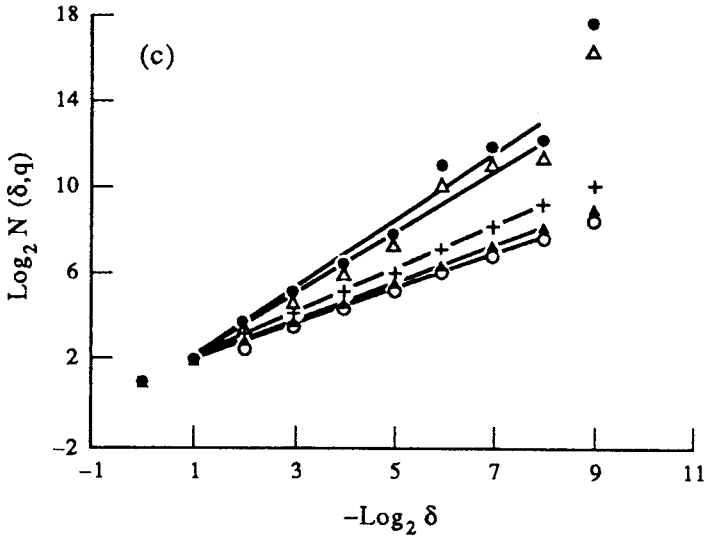
(c)
Log2 N (δ,q)
−Log2 δ
18
14
10
6
2
−2
−1
1
3
5
7
9
11

Fig. 2(a)–(c).

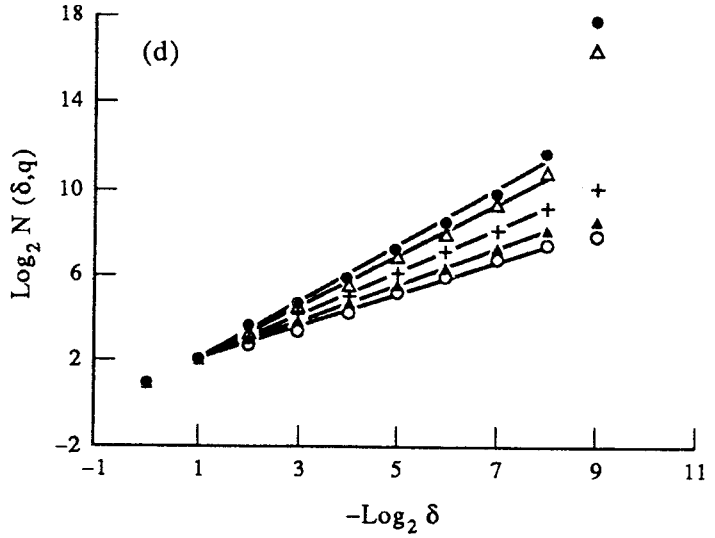

Fig. 2. The multifractal singularity distribution function $F(\alpha)$ *for* C_μ (a) *and* S_μ (b), $\mu = 0.75$ ——, 1.0 – – –, 1.25 . . . . . ; $\mathrm{Log}_2 N(\delta, q)$ as a function of $-\mathrm{Log}_2(\delta)$, for C_1 (c) and S_1 (d), $q = 10$ o o o, 5 ▲ ▲ ▲, 0 + + +, −5 △ △ △, −10 ● ● ●.

represents small values of the range Δ, see (4), and these are more sensitive to the descretization and to cut off errors than the left branch. To the best of our knowledge the behaviour of D_b and $F(\alpha)$ for Riemann's 'non-differentiable' functions are presented here for the first time.

Next we will examine the above results in light of the three properties of Riemann's functions mentioned in our Introduction.

Property 1. R_μ is not differentiable at any irrational point for any $\mu \in (\frac{1}{2}, \frac{5}{4})$.

The most probable singularity of each of the curves in Fig. 2(a) and (b) is given by α_0, the value of the LH exponent α for which $F(\alpha) = 1$. The variation of α_0 as a function of μ, for C_μ and S_μ, is given in Fig. 3. From this figure it is evident that $\alpha_0 < 1$ for $\mu < 1.25$, for both C_μ and S_μ which assures their being non-differentiable almost everywhere; in accordance with Property 1.

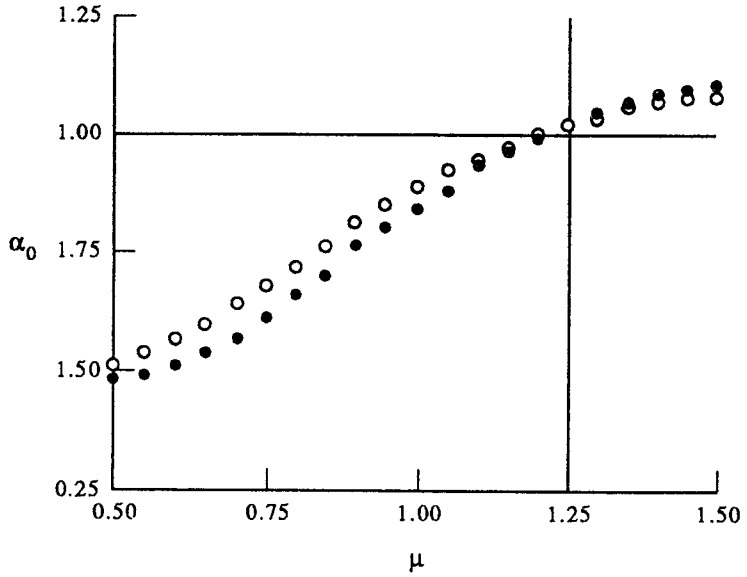

Fig. 3. The most probable L–H exponent α_0 as a function of μ for $C\mu$ o o o, and S_μ ● ● ●.

Property 2. R_μ satisfies uniformly a Hölder condition with regularity exponent $(\mu - \frac{1}{2})$ for $\mu \in (\frac{1}{2}, \frac{3}{2})$.

The strongest singularity is given by the smallest value of the LH exponent, denoted $\alpha_{\min}$. In Fig. 4 we show the variation of $\alpha_{\min}$ as a function of μ, as well as the line $\alpha = \mu - \frac{1}{2}$. Property 2 requires $\alpha_{\min} \geqslant \mu - \frac{1}{2}$, which our calculation found to be true only for $\mu < 1.0$. At present, we have no explanation for the discrepancy at $\mu > 1$.

Property 3. R_μ is differentiable on the dense set of points given by $x = (2P + 1)(2Q + 1)$, P, Q integers for $\mu > \frac{3}{4}$.

This property is related to the fact that the $F(\alpha)$ curves in Fig. 2(a) and (b) extend to $\alpha > 1$. The frequency of occurrence of these regular points is related to $F_r = F(\alpha = 1)$, to be called the dimension of the dust of regular points and shown in Fig. 5. From the figure

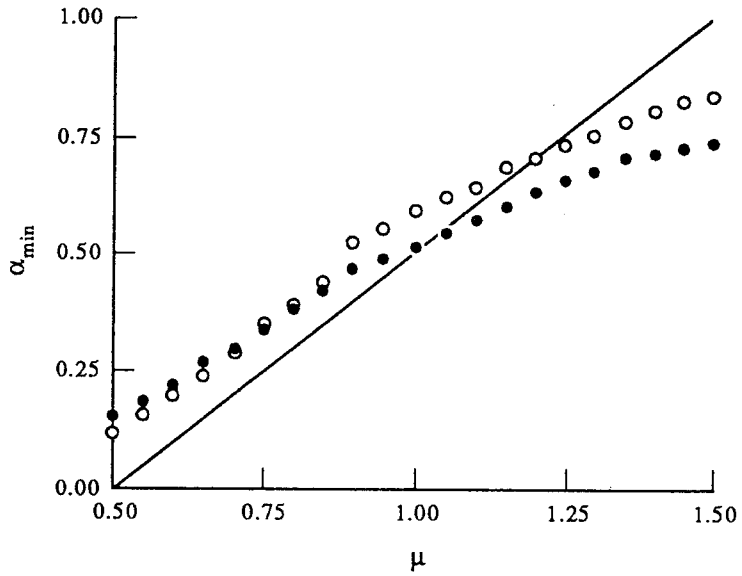

Fig. 4. The strongest singularity exponent $\alpha_{\min}$ as a function of μ for C_μ o o o, S_u • • •.

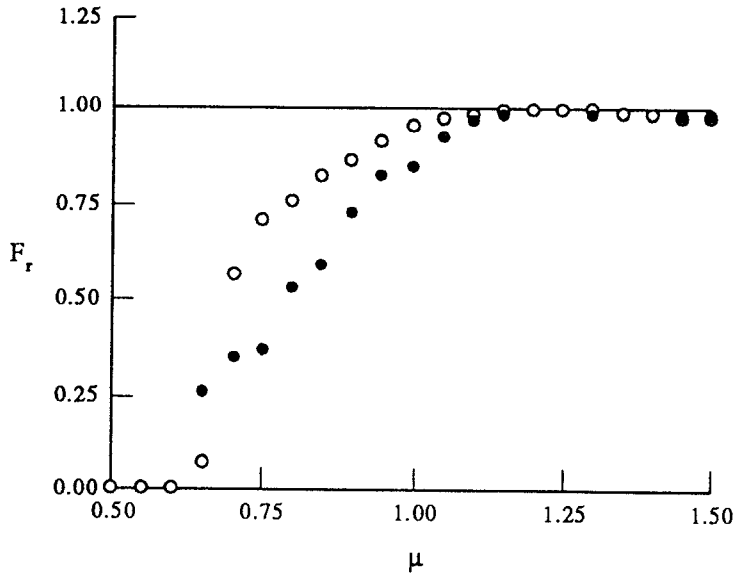

Fig. 5. The dimension of the dust of regular points F_r as a function of μ for C_μ o o o, and S_μ • • •.

one can see that our numerical procedure indicates that regular points exist for $\mu > 0.65$ (they do not exist for $\mu < 0.65$ where $F_r = 0$); which is probably related to the above $\mu = \frac{3}{4}$ value.

Acknowledgements—Michael Stiassnie acknowledges the support of the Science and Engineering Research Council, Grant No: GR/H94894-S23603. He is grateful to Professor S. J. Hogan and the staff of the Department of Engineering Mathematics, University of Bristol, for their hospitality.

REFERENCES

1. M. Holschneider and P. Tchamitchian, Pointwise analysis of Riemann's "non differentiable" function, *Inventiones Mathematical* **105**, 157–175 (1991).
2. B. J. West, *Fractal Physiology and Chaos in Medicine*, World Scientific, Singapore (1990).